Experimental axial force identification based on modified Timoshenko beam theory

Dong-sheng Li[*], Yong-qiang Yuan[a], Kun-peng Li[b] and Hong-nan Li[c]

State Key Laboratory of Coastal and Offshore Engineering, Dalian University of Technology, Dalian, 116024, China

Abstract. An improved method is presented to estimate the axial force of a bar member with vibrational measurements based on modified Timoshenko beam theory. Bending stiffness effects, rotational inertia, shear deformation, rotational inertia caused by shear deformation are all taken into account. Axial forces are estimated with certain natural frequency and corresponding mode shape, which are acquired from dynamic tests with five accelerometers. In the paper, modified Timoshenko beam theory is first presented with the inclusion of axial force and rotational inertia effects. Consistent mass and stiffness matrices for the modified Timoshenko beam theory are derived and then used in finite element simulations to investigate force identification accuracy under different boundary conditions and the influence of critical axial force ratio. The deformation coefficient which accounts for rotational inertia effects of the shearing deformation is discussed, and the relationship between the changing wave speed and the frequency is comprehensively examined to improve accuracy of the deformation coefficient. Finally, dynamic tests are conducted in our laboratory to identify progressive axial forces of a steel plate and a truss structure respectively. And the axial forces identified by the proposed method are in good agreement with the forces measured by FBG sensors and strain gauges. A significant advantage of this axial force identification method is that no assumption on boundary conditions is needed and excellent force identification accuracy can be achieved.

Keywords: axial force identification; modified Timoshenko beam theory; truss structure; dynamic test

1. Introduction

One-dimensional structural members are widely used in civil engineering, e.g., in truss girders or space truss structures. During the construction and service life of these structures, experimental identification of axial forces in these members is of great significance to estimate the internal force redistribution under changing loads or to further learn structural degradation (Li *et al.* 2016). Previous methods can be used to estimate axial force in a bar, e.g. wave-based method (Barnes 2009), magneto-elastic method (Chen *et al.* 2008) and vibration-based method (Irvine *et al.* 1972, 1992). Owing to convenient excitation devices and broad applicability, vibration-based methods

---

[*]Corresponding author, Associate Professor, E-mail: dsli@dlut.edu.cn
[a] MSc. student, E-mail: 573951451@qq.com
[b] MSc. student, E-mail: 930049729@qq.com
[c] Professor, E-mail: hnli@dlut.edu.cn

are most widely utilized techniques for site assessment of member axial forces.

Vibration methods are based on the second-order effect of axial force on the transversal stiffness of a bar. In this sense, a bar is usually recognized as a beam considering its transversal vibration. Hereinafter, both terms are then used interchangeably without distinction. Modal characteristics of a bar depend on its bending stiffness, and are indirectly influenced by the axial force. Practical formulas (Russell 1998) were proposed to estimate the axial force in a bar by considering bending stiffness on the basis of a single natural frequency. Other methods take advantage of vibration responses, measured at several points distributed along the entire structure (Greening and Lieven 2003), or a local vibration measurement along the bar of interest (Tullini and Laudiero 2008). These methods all rely on the assumption of fixed or hinged end boundary conditions of a bar. Very often, however, support conditions are not completely fixed or hinged, but in an in-between state, which will lead to significant force identification errors with arbitrarily assumed boundary conditions. To account for the effect of boundary rotational stiffness, Yamagiwa (Yamagiwa *et al.* 1999) and Mehrabi (Mehrabi *et al.* 1998) proposed an approach to identify the tensile force of inclined cables. As an alternative to analytical formulations, Tullini and Laudiero (2008) made use of one natural frequency and the corresponding modal displacements at three points. The axial force as well as the end flexural stiffness can be recognized under the assumption of infinite translational stiffness at the beam ends. However, such accurate information on the boundary conditions is often not available in practice. In order to solve this situation, Li *et al.* (2013) develop an analytical approach to estimate the axial force in a beam from natural frequency and its corresponding mode shape without assumptions on the boundaries. The above discussed methods are all based on simple Euler-Bernoulli beam theory. They are not appropriate if effects of rotational inertia and/or shear deformation are significant. Furthermore, the inertia of sensors cannot always be neglected (Zui *et al.* 2002). Based on classical Timoshenko beam theory, Maes *et al.* (2013) proposed an axial force method that takes rotational inertia, shear deformation and the mass of the sensors into account. However, the moment of inertia caused by shear deformation is not considered in the classical Timoshenko beam theory (Timoshenko *et al.* 1970), which is also long known to suffer from the second spectrum problem (Stephen 2006). In this work, a modified Timoshenko beam approach (with only one spectrum) is adopted to identify axial forces with improved accuracy.

In this paper, we present the modified Timoshenko beam theory with the inclusion of the axial force as well as the associated member mass and stiffness matrices. The relationship between the changing wave speed and the frequency is examined to improve accuracy of the deformation coefficient as compared to that used in conventional Timoshenko theory. Characteristic equation and steps for axial force identification is thus detailed. Then, numerical simulation is employed to identify axial forces of a beam with various boundary conditions and critical axial force ratios. Finally, dynamic tests are conducted in our laboratory to identify progressive axial forces of a steel plate and a truss structure with the proposed method, and the force identification accuracy with the proposed method is validated.

2. Theoretical background

2.1 Modified Timoshenko beam theory and the deformation coefficient

The free-vibration equation of motion for modified Timoshenko beam under axial force N can

be written as, (Chen *et al.* 2005)

$$EI\frac{\partial^4 v}{\partial x^4} + \frac{NEI}{k_y GA}\frac{\partial^4 v}{\partial x^4} - \eta\rho I\frac{\partial^4 v}{\partial x^2 \partial t^2} - N\frac{\partial^2 v}{\partial x^2} - \frac{\rho EI}{k_y G}\frac{\partial^4 v}{\partial t^2 \partial x^2} + \rho A\frac{\partial^2 v}{\partial t^2} = 0 \tag{1}$$

In the equation, $v(x,t)$ is the transverse-displacement response varying with position x and time t, k_y is the shear deformation coefficient. The axial force N is positive for a tensile force and negative for a compressive force. The geometric moment of inertia I, cross section A, and material density ρ are assumed to be known. The deformation coefficient η is a non-dimensional parameter considering the effect of non-rigid body rotation inertia as follows,

$$\eta = \frac{1}{2}\left[1 - \frac{E}{k_y G} - \frac{A}{I\left(\frac{\omega}{c'}\right)^2} + \sqrt{\left(1 + \frac{E}{k_y G} + \frac{A}{I\left(\frac{\omega}{c'}\right)^2}\right)^2 - 4\frac{E}{k_y G}}\right] \tag{2}$$

where, c' is the wave speed which varies with wave number, ω is the angular frequency.

The deformation coefficient η plays an essential role in the modified Timoshenko beam theory since it determines how to account for rotational inertia due to the shearing deformation of each beam cross section. Conventionally, the deformation coefficient η takes the non-rigid nature of deformed beam section under the influence of shearing force into consideration with a fixed shear wave speed, and is obtained by equating the first natural frequency with classical Timoshenko theory (Timoshenko *et al.* 1970) to that with modified Timoshenko beam theory (Chen *et al.* 2005).

In fact, the wave speed is increasing with beam vibrating frequency until it reaches the fixed shear wave speed. If a constant wave speed is used even in the low frequency domain, the deformation coefficient will be exaggerated. To account for this effects, the relationship between the changing wave speed and the frequency is examined as follows (Jean-Louis *et al.* 2006)

$$EI\frac{\partial^4 v}{\partial x^4} - \rho I\frac{\partial^4 v}{\partial x^2 \partial t^2} - \frac{\rho EI}{k_y G}\frac{\partial^4 v}{\partial t^2 \partial x^2} + \rho A\frac{\partial^2 v}{\partial t^2} + \frac{\rho^2 I}{k_y G}\frac{\partial^4 v}{\partial t^4} = 0 \tag{3}$$

Solving Eq. (3) under free vibration by assuming the basic solution

$$v(x,t) = \psi e^{i(kx - \omega t)} \tag{4}$$

where, ψ is wave amplitude, k is wave number and is given by

$$k = \frac{\omega}{c'} \tag{5}$$

By introducing Eq. (4) into Eq. (3), the wave number k is obtained as

$$k = \sqrt{\frac{\left(\frac{I}{A} + \frac{EI}{k_y GA}\right)\omega^2 + \sqrt{\left(\left(\frac{I}{A} + \frac{EI}{k_y GA}\right)\omega^2\right)^2 - 4\frac{EI}{\rho A}\left(\frac{\rho I}{k_y GA}\omega^4 - \omega^2\right)}}{2\frac{EI}{\rho A}}} \tag{6}$$

By introducing Eqs. (4) and (5) into Eq. (3), the wave speed c' is obtained as

$$c' = \sqrt{\frac{\left(\left(\frac{I}{A} + \frac{EI}{k_y GA}\right)k^4 + k^2\right) \pm \sqrt{\left(\left(\frac{I}{A} + \frac{EI}{k_y GA}\right)k^4 + k^2\right)^2 - 4\frac{EI}{\rho A}\frac{\rho I}{k_y GA}k^8}}{2\frac{\rho I}{k_y GA}k^4}} \tag{7}$$

To examine the different influence of fixed shear wave speed $\sqrt{(G/\rho)}$ and varying wave speed c' on the deformation coefficient, a simple steel bar is selected for the purpose of demonstration. The steel bar has a circular cross section with a diameter 0.014 m. The shear deformation coefficient k_y is taken as $3/4$. Density ρ, Young's modulus E, Shear modulus G and Poisson's ratio μ are taken as $7.93 \times 10^3 \text{kg/m}^3$, $1.93 \times 10^{11} \text{N/m}^2$, $E/[2(1+\mu)]$ and 0.3, respectively. The longitudinal wave speed and shear wave speed are taken as $\sqrt{(E/\rho)}$ and $\sqrt{(G/\rho)}$. By introducing these parameters into Eq.(7), the relation between c' and k is shown in Fig. 1.

The first wave speed of classical Timoshenko beam theory is zero and the second speed is infinity when the wave number equals to zero as shown in Fig. 1. The first wave speed is traditionally considered right and it increases to shear wave speed when wave number increases gradually (Guyader *et al.* 2006).

Shear wave speed and varying wave speed of the classical Timoshenko beam are then both used to calculate deformation coefficient as shown in Fig. 2. As the angular frequency increases, both deformation coefficients η decrease. The deformation coefficients η obtained from varying wave speed by the classical Timoshenko beam theory is smaller than η from fixed shear wave speed when angular frequency is not large enough as discussed in preceding paragraph. Therefore, it is recommended to use varying wave speed to calculate deformation coefficient η instead of fixed shear wave speed.
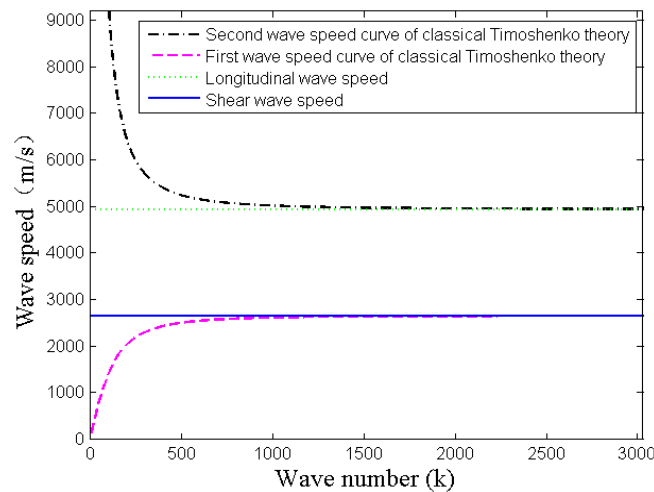
Fig. 1 The relationship between wave speed and wave number in the classical Timoshenko beam
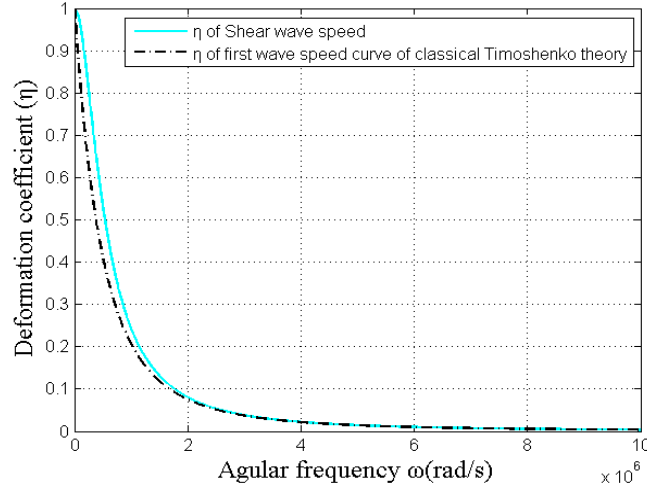
Fig. 2 The relation of deformation coefficient η and angular frequency

2.2 Consistent mass and stiffness element for modified Timoshenko beam theory

For the purpose of numerical simulation, the influence of boundary conditions and slenderness on the accuracy of axial force identification, element mass and stiffness matrices are needed for the modified Timoshenko beam theory. As proposed by Friedman and Kosmatka (1993) to avoid shear lock, two shape functions are used to obtain associated member mass and stiffness matrices

$$[\mathbf{N_v}]^{\mathbf{T}} = \begin{bmatrix} \frac{1}{(1+\phi)}\left\{2\left(\frac{x}{l}\right)^3 - 3\left(\frac{x}{l}\right)^2 - \phi\left(\frac{x}{l}\right) + (1+\phi)\right\} \\ \frac{1}{(1+\phi)}\left\{\left(\frac{x}{l}\right)^3 - \left(2+\frac{\phi}{2}\right)\left(\frac{x}{l}\right)^2 + \left(1+\phi\right)\left(\frac{x}{l}\right)\right\} \\ -\frac{1}{(1+\phi)}\left\{2\left(\frac{x}{l}\right)^3 - 3\left(\frac{x}{l}\right)^2 - \phi\left(\frac{x}{l}\right)\right\} \\ \frac{1}{(1+\phi)}\left\{\left(\frac{x}{l}\right)^3 - \left(1-\frac{\phi}{2}\right)\left(\frac{x}{l}\right)^2 + \frac{\phi}{2}\left(\frac{x}{l}\right)\right\} \end{bmatrix} \tag{8}$$

$$[\mathbf{N_\theta}]^{\mathbf{T}} = \begin{bmatrix} \frac{6}{(1+\phi)l}\left\{\left(\frac{x}{l}\right)^2 - \left(\frac{x}{l}\right)\right\} \\ \frac{1}{(1+\phi)}\left\{3\left(\frac{x}{l}\right)^3 - (4+\phi)\left(\frac{x}{l}\right) + (1+\phi)\right\} \\ -\frac{6}{(1+\phi)}\left\{\left(\frac{x}{l}\right)^2 - \left(\frac{x}{l}\right)\right\} \\ \frac{1}{(1+\phi)}\left\{3\left(\frac{x}{l}\right)^3 - (2-\phi)\left(\frac{x}{l}\right)\right\} \end{bmatrix} \tag{9}$$

in which the ratio of the beam bending stiffness to the shear stiffness, ϕ, is defined as

$$\phi = \frac{12EI}{GAl^2 k_y} \tag{10}$$

According to Williams and Wittrick (1970), energy function Π (Eq. (11)) can be obtained by using the minimum potential principle, and the first variation of Eq. (11) is equal to zero.

$$\Pi = -\sum_{i=1}^{4} v_i^B F_i^B + \int_0^l \left[\frac{1}{2} \left(EI + \frac{NEI}{GAk_y} \right)(v'')^2 + \frac{1}{2} \left(\eta \rho I \omega^2 - N + \frac{\rho EI}{Gk_y} \omega^2 \right)(v')^2 + \rho A \ddot{v} v \right] dx \tag{11}$$

By substituting the shape function Eqs. (9) and (10) into Eq. (11) and letting its first variation equal to zero the stiffness matrix is found

$$\mathbf{K} = \frac{EI}{(1+\phi)l^3} \begin{bmatrix} 12 & 6l & -12 & 6l \\ 6l & (4+\phi)l^2 & -6l & (2-\phi)l^2 \\ -12 & -6l & 12 & -6l \\ 6l & (2-\phi)l^2 & -6l & (4+\phi)l^2 \end{bmatrix} + N \begin{bmatrix} \frac{6}{5l} & \frac{1}{10} & -\frac{6}{5l} & \frac{1}{10} \\ \frac{1}{10} & \frac{2l}{15} & -\frac{1}{10} & -\frac{l}{30} \\ -\frac{6}{5l} & -\frac{1}{10} & \frac{6}{5l} & -\frac{1}{10} \\ \frac{1}{10} & -\frac{l}{30} & -\frac{1}{10} & \frac{2l}{15} \end{bmatrix} \tag{12}$$

The first term in Eq. (12) is the classical stiffness matrix for the Timoshenko beam theory, and will reduce to the stiffness matrix for the Bernoulli-Euler theory be setting ($\phi = 0$). The second term of the stiffness matrix in Eq. (12) appears due to the second-order effect of the axial force on the transversal stiffness.

In a similar way, the consistent mass matrix can be found as

$$[\mathbf{M}] = \frac{\rho A l}{210(1+\phi)^2} [\mathbf{M}_{\rho A}] + \frac{\eta \rho I}{30(1+\phi)^2 l} [\mathbf{M}_{\rho I}] \tag{13}$$

$$[\mathbf{M}_{\rho A}] = \begin{bmatrix} (70\phi^2 + 147\phi + 78) & & & \text{sysmetric} \\ (35\phi^2 + 77\phi + 44)\frac{l}{4} & (70\phi^2 + 147\phi + 78)\frac{l^2}{4} & & \\ (35\phi^2 + 63\phi + 27) & (35\phi^2 + 63\phi + 26)\frac{l}{4} & (70\phi^2 + 147\phi + 78) & \\ -(35\phi^2 + 63\phi + 26)\frac{l}{4} & -(7\phi^2 + 14\phi + 6)\frac{l^2}{4} & -(35\phi^2 + 77\phi + 44)\frac{l}{4} & (70\phi^2 + 147\phi + 78)\frac{l^2}{4} \end{bmatrix}$$

$$[\mathbf{M}_{\rho I}] = \begin{bmatrix} 36 & & & \text{symmetric} \\ -(15\phi - 3)l & (10\phi^2 + 5\phi + 4)l^2 & & \\ -36 & (15\phi - 3)l & 36 & \\ -(15\phi - 3)l & (5\phi^2 - 5\phi - 1)l^2 & (15\phi - 3)l & (10\phi^2 + 5\phi + 4)l^2 \end{bmatrix} \tag{14}$$

The first term of the mass matrix in Eq. (13) attributes to the inertia of translational movement, whereas the second term is associated with rotational inertia. These two matrices will reduce to the

consistent translational and rotatory mass matrices for the Bernoulli-Euler beam theory by setting ($\phi = 0$). With both stiffness and mass matrices derived with the modified Timoshenko beam theory in Eq. (1), more accurate natural frequencies and mode shapes of a beam can be obtained, which will be used in the numerical simulations in subsequent section 3.

2.3 Characteristic equation for axial force identification

For axial force identification, Eq. (1) can be solved by separating different variables by assuming the transverse-displacement response $v(x,t)$ to be harmonic at a certain frequency ω

$$v(x,t) = \varphi(x)\sin(\omega t) \tag{15}$$

By introducing Eq. (15) into Eq. (1), the following equation is obtained

$$a\frac{d^4\varphi(x)}{dx^4} + b\frac{d^2\varphi(x)}{dx^2} + c\varphi(x) = 0 \tag{16}$$

in which, the parameters a, b and c are given by

$$a = EI(1 + \frac{N}{k_y GA})$$

$$b = \eta\rho I\omega^2 + \frac{E\rho I\omega^2}{k_y G} - N$$

$$c = -\rho A\omega^2 \tag{17}$$

The solution of Eq. (16) s then given by

$$\varphi(x) = \sum_{k=1}^{4} C_k \exp(\beta_k x) \tag{18}$$

where

$$\beta_1 = \sqrt{\frac{-b + \sqrt{b^2 - 4ac}}{2a}} \qquad \beta_2 = -\sqrt{\frac{-b + \sqrt{b^2 - 4ac}}{2a}}$$

$$\beta_3 = \sqrt{\frac{-b - \sqrt{b^2 - 4ac}}{2a}} \qquad \beta_4 = -\sqrt{\frac{-b - \sqrt{b^2 - 4ac}}{2a}} \tag{19}$$

The parameters $\beta_k (k = 1,,,4)$ depend both on the bar properties and the axial force N. The coefficients $C_k (k = 1,,,4)$ depend on the boundary conditions. There are, in total, five unknowns (C_1, C_2, C_3, C_4, N) in Eq. (18). Consequently, at least five equations are needed to solve the non-linear Eq. (18) in order to identify the axial force. Fortunately, this condition can be easily fulfilled by measuring certain natural frequency ω and modal displacement at five points along a beam/bar.

Due to the non-linear nature of the solution in Eq. (18), the axial force has to be estimated in an iterative fashion. For a given value of frequency ω, the parameters a, b and c depend only on the axial force N. Once the axial force N is assumed to be a given value and modal displacement at five points are obtained (Maes 2013), the ratio λ_{ij} of two points displacement is given by

$$\lambda_{ij} = \frac{\varphi(x_i)}{\varphi(x_j)} = \frac{C_1 \exp(\beta_1 x_i) + C_2 \exp(\beta_2 x_i) + C_3 \exp(\beta_3 x_i) + C_4 \exp(\beta_4 x_i)}{C_1 \exp(\beta_1 x_j) + C_2 \exp(\beta_2 x_j) + C_3 \exp(\beta_3 x_j) + C_4 \exp(\beta_4 x_j)} \tag{20}$$

which can be further transformed to

$$(\exp(\beta_1 x_i) - \lambda_{ij} \exp(\beta_1 x_j))C_1 + (\exp(\beta_2 x_i) - \lambda_{ij} \exp(\beta_2 x_j))C_2$$
$$+ (\exp(\beta_3 x_i) - \lambda_{ij} \exp(\beta_3 x_j))C_3 + (\exp(\beta_4 x_i) - \lambda_{ij} \exp(\beta_4 x_j))C_4 = 0 \tag{21}$$

Four different ratios from modal displacement leads to the characteristic equation as follows

$$\begin{bmatrix} \exp(\beta_1 x_1) - \lambda_{12}\exp(\beta_1 x_2) & \exp(\beta_2 x_1) - \lambda_{12}\exp(\beta_2 x_2) & \exp(\beta_3 x_1) - \lambda_{12}\exp(\beta_3 x_2) & \exp(\beta_4 x_1) - \lambda_{12}\exp(\beta_4 x_2) \\ \exp(\beta_1 x_1) - \lambda_{13}\exp(\beta_1 x_3) & \exp(\beta_2 x_1) - \lambda_{13}\exp(\beta_2 x_3) & \exp(\beta_3 x_1) - \lambda_{13}\exp(\beta_3 x_3) & \exp(\beta_4 x_1) - \lambda_{13}\exp(\beta_4 x_3) \\ \exp(\beta_1 x_1) - \lambda_{14}\exp(\beta_1 x_4) & \exp(\beta_2 x_1) - \lambda_{14}\exp(\beta_2 x_4) & \exp(\beta_3 x_1) - \lambda_{14}\exp(\beta_3 x_4) & \exp(\beta_4 x_1) - \lambda_{14}\exp(\beta_4 x_4) \\ \exp(\beta_1 x_1) - \lambda_{15}\exp(\beta_1 x_5) & \exp(\beta_2 x_1) - \lambda_{15}\exp(\beta_2 x_5) & \exp(\beta_3 x_1) - \lambda_{15}\exp(\beta_3 x_5) & \exp(\beta_4 x_1) - \lambda_{15}\exp(\beta_4 x_5) \end{bmatrix} \begin{bmatrix} C_1 \\ C_2 \\ C_3 \\ C_4 \end{bmatrix} = 0 \tag{22}$$

Which can be simplified as

$$S_{4\times4} \begin{bmatrix} C_1 \\ C_2 \\ C_3 \\ C_4 \end{bmatrix} = 0 \tag{23}$$

where S is the characteristic matrix. As boundary conditions must have non-zero solution, the determinant of the characteristic matrix S should be equal to zero

$$|S| = 0 \tag{24}$$

For the true value of the axial force N, the value of $|S|$ approaches zero, by which actual axial force can be determined.

Also Eq. (18) can be rewritten as

$$\mathbf{Q} = \mathbf{Ac} \tag{25}$$

The vector $\mathbf{Q}(\in \mathrm{R}^{n\times1})$ contains the modal response φ at each sensor position. The vector $\mathbf{c}(\in \mathrm{R}^{4\times1})$ involves the four coefficients C_k which are to be determined. The coefficient matrix $\mathbf{A}$ is given by the form

$$\mathbf{A} = \begin{bmatrix} \exp(\beta_1 x_1) & \exp(\beta_2 x_1) & \exp(\beta_3 x_1) & \exp(\beta_4 x_1) \\ \exp(\beta_1 x_2) & \exp(\beta_2 x_2) & \exp(\beta_3 x_2) & \exp(\beta_4 x_2) \\ \vdots & & & \\ \exp(\beta_1 x_n) & \exp(\beta_2 x_n) & \exp(\beta_3 x_n) & \exp(\beta_4 x_n) \end{bmatrix} \tag{26}$$

In a least squares sense, the value of $\mathbf{c}$ can be obtained as

$$\mathbf{c} = \mathbf{A}^\dagger \mathbf{Q} \tag{27}$$

where $\mathbf{A}^\dagger$ is the pseudo inverse of the coefficient matrix $\mathbf{A}$.

In such a way, boundary conditions and axial forces can be simultaneously identified.

The force identification procedure is as follows:1) The ratio λ_{ij} is computed according to Eq. (20) with identified modal displacement at two points; 2) The characteristic matrix S is constructed with the different ratios λ_{ij}; 3) Compute determinant of the characteristic matrix S by assuming different axial forces N, and actual axial force can be determined when the determinant equals zero.

3. Numerical simulation

The axial force estimation procedure presented in section 2 is illustrated for the case of a beam with rectangular cross section as shown in Fig. 3. To ascertain the accuracy and the applicability of the proposed method, parameters of the beam in the paper (Li *et al.* 2013) are utilized for the purpose of comparison, in which Euler-Bernoulli beam theory was adopted. The beam is of an identical steel member with a length L of 0.72 m, width b of 0.035 m and height h of 0.005m . The shear deformation coefficient k_y is taken as 5/6. Density ρ, Young's modulus E and Poisson's ratio μ are taken as 7860 kg/m^3, 2.1×10^{11}N/m^2 and 0.3, respectively. Five sensors (Wang *et al.* 2017) are uniformly attached along the beam (Fig. 1, S_k (k=1…5)) and the mass of each sensor is 0.01 kg. The beam is subjected to a static axial force of 15 kN. A finite element (FE) model is developed with the stiffness and mass matrices derived in Eqs. (12)-(14) in MATLAB. For all cases, the element size is set to 0.012 m.

3.1 Determination of boundary conditions

The mode shapes calculated by the FE model are extracted at the five sensor locations. The sensor S_3 is taken as a reference sensor and the others as regular sensors. Four different boundary conditions are investigated to examine the effectiveness of the proposed method as shown in Table 1.
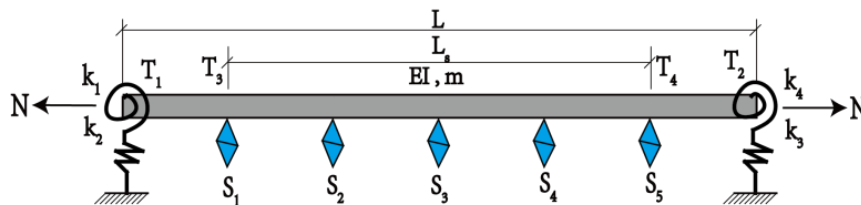
Fig. 3 Dynamic test model of a bar

Table 1 Axial force identification with four different boundary conditions

Case	K_1 (N/m^{-1})	K_2 (Nm/rad^{-1})	K_3 (N/m^{-1})	K_4 (Nm/rad^{-1})	N_E (kN)	N_M (kN)	Error reduced (%)
A_1	∞	∞	∞	∞	15.165	15.017	0.987
A_2	∞	0	∞	0	15.122	15.028	0.627
A_3	∞	1000	∞	1000	14.829	15.041	0.867
A_4	∞	0	2000	0	15.088	15.028	0.4

In Table 1, $K_i (i = 1,2,3,4)$ are the support stiffness at the boundaries. In the first case, A1, both ends of the beam are fixed for two degrees of freedoms (DOFs) ($K_1 = K_2 = K_3 = K_4 = \infty$). In the second case, A2, both ends of the beam are fixed in the horizontal direction ($K_1 = K_3 = \infty$) but free for rotation ($K_2 = K_4 = 0$). In the third case, A3, both ends of the beam are fixed in the horizontal direction ($K_1 = K_3 = \infty$) but limited with given rotation stiffness ($K_2 = K_4 = 1000$ Nm/rad^{-1}). In the fourth case, A4, the beam is fixed in the horizontal direction ($K_1 = \infty$) at the left end, but limited with given horizontal stiffness ($K_3 = 2000$ Nm/rad^{-1}) at the right end, and free for rotation at both ends.

Identified axial force based on the first five bending modes are shown in Table 1 along with identification errors. In Table 1, N_E is the axial force identified by Li *et al.* (2013) with the Euler-Bernoulli beam theory, whereas N_M is the axial force estimated by the modified Timoshenko beam theory as proposed in Section 2. For each of the four cases, improved force identification results are achieved by the modified Timoshenko beam theory with an accuracy almost up to 1%, which is better than those obtained with the Euler-Bernoulli beam theory.

3.2 Axial force identification with different ξ

A non-dimensional parameter ξ is usually defined to evaluate the effect of bending stiffness on the free vibration of beam member in previous studies (Mehrabi *et al.* 1998)

$$\xi = L\sqrt{\frac{N}{EI}} \tag{28}$$

When axial force is compressive

$$\xi = \pi\sqrt{\frac{N}{N_{crE}}} \quad \text{with} \quad N_{crE} = \frac{\pi^2 EI}{L^2} \tag{29}$$

Li *et al.* (2013) mainly concentrate on the range of $\xi \leq 50$, and axial forces cannot be identified in some cases in the range of $\xi \geq 50$. This section will take the non-dimensional parameter, critical axial force ratio, ξ, into consideration. In Table 2, E is the Young's modulus of the beam with a value of 210 GPa for all five cases; L, b, and h are the length, width and height of the beam, respectively; N is the axial force applied on the beam; N_E is the axial force identified by Li *et al.*

(2013) with the Euler-Bernoulli beam theory, whereas N_M is the axial force estimated by the modified Timoshenko beam theory proposed in Section 2.

There are in total five cases with different beam dimensions (B1, B2, …, B5) and resulting with various critical axial force ratio ξ, ranging from 1.036 to 56.338 as shown in Table 2. The estimated axial forces for five cases with the first 5 bending modes are listed in Table 2. For cases, B1, B2 and B4, both Euler-Bernoulli beam theory and the modified Timoshenko beam theory can yield accurate axial force estimation. However, conventional Euler-Bernoulli beam theory failed for cases B3 and B5, whereas the modified Timoshenko beam theory can still yield accurate axial force estimation although the accuracy of identified forces is decreasing a bit with the increase of the non-dimensional parameter ξ. Therefore, the proposed method has a wider range of applicability than conventional Euler-Bernoulli beam theory.

4. Experimental validation

In this section, the effectiveness of the proposed axial force identification method with modified Timoshenko beam theory is further investigated by laboratory tests of a steel beam.

4.1 Experiment setup

The dimensions and physical properties of the steel beam specimen are listed in Table 3. Five PCB LC0101 miniature piezoelectric accelerometers (sensitivity 0.1 V/g, mass 8 g), with micro IC amplifier built-in, are glued to the surface of the steel beam at even distances as shown in Fig. 2. The accelerometers are respectively numbered as $S1, S2, S3, S4, S5$ from top to bottom.

The measurement frequency ranges from 0.5 to 8000 Hz. Both ends of the specimen are fixed into the MTS810 (Su 2006) material servo instrument with the TestStar IIs control system provided by the MTS company. The MTS810 and the control terminal of TestStar IIs system are shown in Fig. 3. The specimen is axially loaded increasingly by uniaxial tension force from 0 kN to 30 kN with a step increment of 5 kN.

Table 2 Axial force identification with different ξ

Case	E (N/m^2)	L (m)	b (m)	h (m)	N (kN)	ξ	N_E (kN)	N_M (kN)	Error reduced (%)
B$_1$		0.72	0.08	0.012	5	1.036	5.009	5.001	0.16
B$_2$		0.72	0.035	0.005	5	5.843	5.0	5.0	0.0
B$_3$		1.2	0.035	0.005	5	9.697	*	5.0	*
B$_4$	2.10E+11	0.72	0.035	0.005	30	14.52	30.0	30.0	0.0
B$_5$		0.72	0.035	0.002	30	56.338	*	29.948	*

Fig. 4 Experimental specimen and sensor locations

(a) The material servo instrument MTS810   (b) The control terminal TestStar IIs

Fig. 5 Experiment equipment for axial force step loading

Table 3 Parameters of experiment bar specimen

N	ξ	L (length)	0.6 m
0 kN	0	b (width)	0.035 m
5 kN	5.734	h(thickness)	0.0045 m
10 kN	8.109	E(Young's Modulus)	2.06×10^{11} N/m^2
15 kN	9.931	G(Shear Modulus)	8.05×10^{10} N/m^2
20 kN	11.468	ρ (density)	8163kg/m^3
25 kN	12.821	μ (Poisson ratio)	0.28
30 kN	14.045	k_y (shear deformation coefficient)	5/6

Fig. 6 Data acquisition instrument of LMS Test.Lab

4.2 Experimental modal identification

A series of impact forces is performed by a hammer on the middle of the beam, close to the accelerometer S3. The LMS (Learning Management System) Test.Lab (Peeters *et al.* 2001) is employed for experimental modal analysis and the front-end acquisition equipment is shown in Fig. 6.

The deterministic-stochastic subspace identification method is adopted for modal analysis with a sampling frequency of 2500 Hz. The beam is excited in the horizontal direction, and the responses are measured horizontally as well. The frequency response function of measured acceleration at the sensor S1 to S3 is plotted in Fig. 7, and a stabilization diagram with apparently five natural frequencies up to around 1000Hz is shown in Fig. 8. Identified first five natural frequencies and mode shapes of the beam are listed in Table 4 when the beam is bearing various axial forces increasing from 0 kN to 30 kN with a step of 5 kN. Identified frequencies are 55.564, 77.508, 91.175, 102.797, 109.456, 124.926, and 138.677 for seven axial loading cases. It is seen obviously that the first natural frequencies is increasing sharply with applied axial forces. Identified mode shapes are listed at the sensor locations from S1 to S5 with S3 as the reference sensor and normalized displacement.
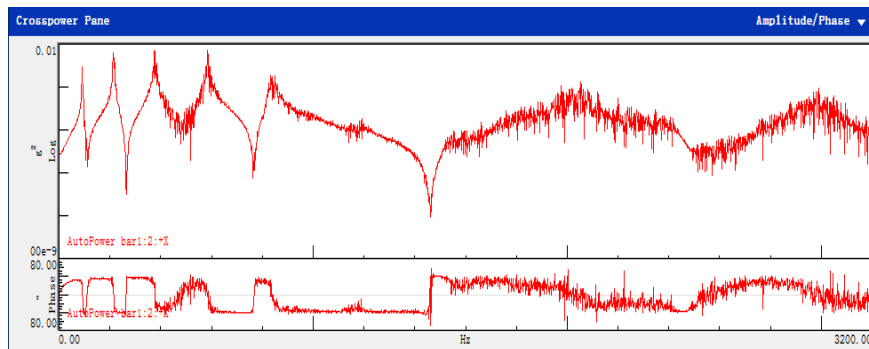
Fig. 7 Measured frequency response function at sensor S1

Table 4 Identified natural frequencies and mode shapes of the beam under various axial forces

N	0 kN	5 kN	10 kN	15 kN	20 kN	25 kN	30 kN
Mode 1							
frequency	55.564	77.508	91.175	102.797	109.456	124.926	138.677
S1	0.361	0.372	0.404	0.402	0.463	0.442	0.425
S2	0.828	0.830	0.846	0.831	0.837	0.921	0.863
S3	1.000	1.000	1.000	1.000	1.000	1.000	1.000
S4	0.801	0.823	0.823	0.811	0.876	0.852	0.835
S5	0.333	0.383	0.388	0.392	0.464	0.430	0.380
Mode 2							
frequency	155.594	186.858	214.194	234.382	253.858	270.608	286.344
S1	-0.799	-0.831	-0.812	-0.831	-0.841	-0.872	-0.899
S2	-0.959	-0.952	-0.925	-0.931	-0.922	-0.931	-0.936
S3	0.043	0.039	0.053	0.003	0.053	0.066	0.072
S4	1.000	1.000	1.000	1.000	1.000	1.000	1.000
S5	0.763	0.782	0.779	0.797	0.815	0.858	0.832
Mode 3							
frequency	309.358	346.687	376.493	402.494	426.607	449.69	470.204
S1	-0.967	-0.989	-0.995	-0.966	-0.967	-0.981	-0.982
S2	-0.294	-0.252	-0.231	-0.246	-0.292	-0.206	-0.220
S3	0.934	0.943	0.962	0.960	0.951	0.968	0.965
S4	-0.230	-0.210	-0.190	-0.174	-0.165	-0.164	-0.167
S5	-1.000	-1.000	1.000	-1.000	-1.000	-1.000	-1.000
Mode 4							
frequency	511.776	550.368	585.615	614.531	641.71	670.342	697.501
S1	-0.931	-0.925	-0.932	-0.965	-0.970	-0.939	-0.917
S2	0.716	0.743	0.847	0.884	0.803	0.788	0.786
S3	0.008	0.083	0.084	0.007	0.068	0.008	0.101
S4	-0.713	-0.726	-0.760	-0.750	-0.762	-0.781	-0.792
S5	1.000	1.000	1.000	1.000	1.000	1.000	1.000
Mode 5							
frequency	763.705	805.49	840.996	872.886	900.571	933.282	971.128
S1	0.888	0.728	0.850	0.721	0.744	0.744	0.742
S2	-0.917	-0.911	-0.920	-0.942	-0.936	-0.919	-0.898
S3	0.963	1.000	1.000	1.000	0.998	1.000	1.000
S4	-1.000	-0.945	-0.968	-0.969	-1.000	-0.953	-0.952
S5	0.882	0.748	0.759	0.740	0.779	0.797	0.664

Examining the stabilization diagram of stochastic subspace modal identification in Fig. 8, the first and second modes are more stabilized with the increase of the rank, which will naturally leads to better modal identification of the first two modes and contribute to the excellent axial force identification results for both modes in Table 5. In fact, only one mode is sufficient to identify the axial force in each case.
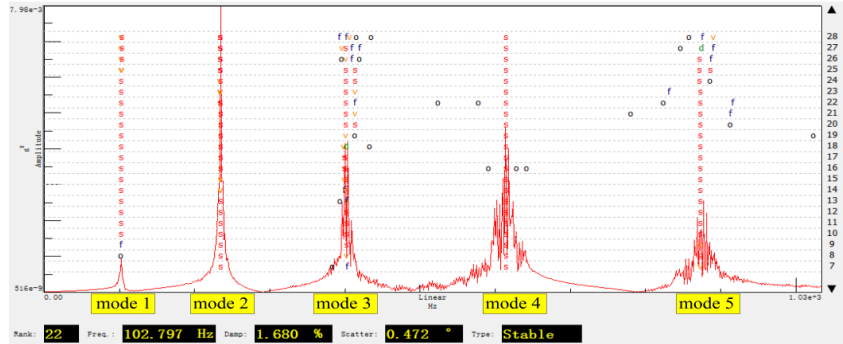
Fig. 8 Stabilization diagram for modal analysis at sensor S1

4.3 Axial force estimation

Considering hinged boundary conditions in our tests, the displacements at both ends of the beam can be regarded as zero. For each of the five modes, the axial tensile force is identified using the modified Timoshenko beam method as developed in Section 2.

The first five modes along with axial force identification results are all presented in Tables 4 and 5 for the comparison of identification accuracy with different modes. The estimated axial forces with the improved Timoshenko beam method are listed in Table 5. The average deviation of estimated axial forces from actual ones falls within the range of 1 kN. For the loading case of 5kN, the errors of axial force estimation are comparatively larger than other loading cases, which may be induced by initial friction effects of the fixtures. For the loading cases of 10~30 kN, the relative force identification errors are comparatively small, especially for the first mode and the second mode.

Table 5 Identification of axial force by improved Timoshenko beam method

N_{true} (kN)	Mode 1		Mode 2		Mode 3		Mode 4		Mode 5	
	N_{id} (kN)	Error (%)	N_{id} (kN)	Error (%)	N_{id} (kN)	Error (%)	N_{id} (kN)	Error (%)	N_{id} (kN)	Error (%)
5	5.51	10.24	4.93	1.40	5.35	7.00	5.05	1.00	5.50	10.00
10	9.81	1.90	10.09	0.9	9.98	0.20	9.53	4.70	10.40	4.00
15	14.79	1.40	14.18	5.47	15.19	1.27	14.43	3.80	15.45	3.00
20	19.81	0.95	19.15	4.25	21.44	7.20	18.98	5.10	20.46	2.30
25	25.13	0.52	24.25	3.0	25.79	3.16	24.29	2.84	24.36	2.56
30	29.85	0.50	29.96	0.13	29.81	0.63	28.72	4.27	30.21	0.70

5. Engineering application

5.1 A truss structure

In this section, the effectiveness of the proposed method is further investigated by identifying the axial forces of a steel truss structure. The truss is made up of circular hollow bar and connected by ball joints. The dimension of the truss is shown in Fig. 9 and the physical properties of the circular hollow bars are listed in Table 6. Two identical single trusses are connected laterally to guarantee its horizontal stability. A steel plate lied on two middle ball joints is employed to distribute the vertical loading evenly on the truss as shown in Fig. 10(a).

5.2 Calibration tests

In order to obtain actual axial force of bar 1 and 2 (which is marked with red in Fig. 9), fiber Bragg grating (FBG) sensors(Minardo *et al.* 2014) and strain gauges(Li *et al.* 2014) are attached on the bars to measure their strains. Calibration tests are conducted before tests to obtain the relationship between axial forces and measured signals from FBG sensors and strain gauge as shown in Fig. 10(b).

Table 6 Bar parameters of the steel truss

L (length)	0.74 m
d_1 (outside diameter)	0.020 m
d_2(inside diameter)	0.010 m
E(Young's Modulus)	2.1×10^{11} N/m^2
G(Shear Modulus)	8.27×10^{10} N/m^2
ρ (density)	7850kg/m^3
μ (Poisson ratio)	0.269
k_y (shear deformation coefficient)	1/2
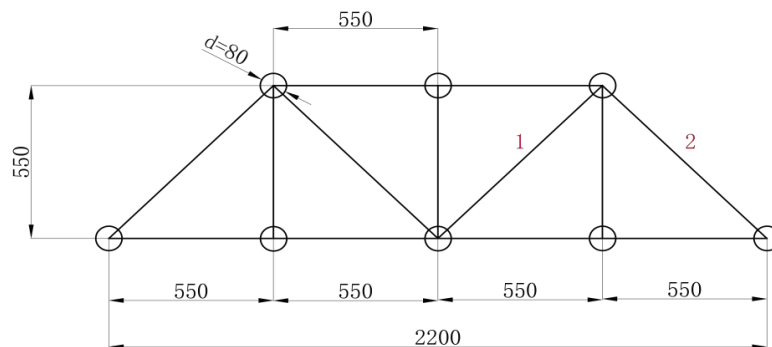
Fig. 9 Dimensions of single truss structure

Table 7 Relationship of Δλ、ΔV and ΔN of bar 1 and 2

relationship expression	Δλ(nm)—ΔN(kN)	ΔV(V)—ΔN(kN)
bar 1	Δλ=0.0250ΔN+0.0038	ΔV=0.0574ΔN+0.0003
bar 2	Δλ=0.0256ΔN-0.0029	ΔV=0.0596ΔN+0.0084
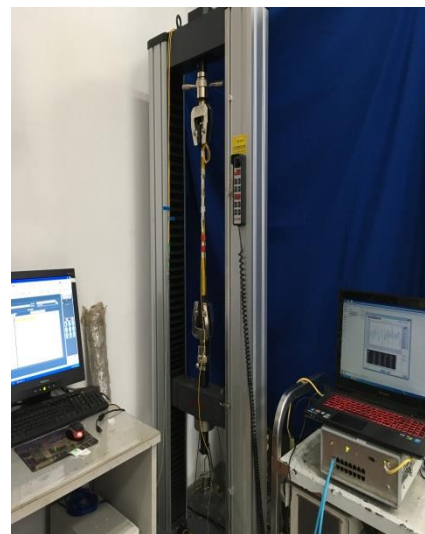
(a) Truss model   (b) Calibration tests of bar 1 and 2

Fig. 10 Experiment model and calibration tests

When the bar 1 and 2 are bearing various axial forces increasing from 0 kN to 10 kN with a step of 1kN for four times, the voltages of strain gauges and wave length changes of FBG sensors can then be measured to obtain the relationship. The relation expression between FBG's wave length variation ($\Delta\lambda$) , strain gauge's voltage variation (ΔV) and axial force variation (ΔN) for two bars are listed in Table 7.

5.3 Axial force identification

The bars was compressively loaded by SNAS10 from 0 kN to 10 kN with a step increment of 2.5 kN. Five PCB LC0101 miniature piezoelectric accelerometers were glued to the surface of the steel bar at even distances as shown in Fig. 11. After each load step, a series of impact forces was performed by a hammer on the middle of the beam, close to the middle accelerometer. The data of acceleration, voltage value and wave length were also recorded.

The first modes of two bars along with different compression load are presented in Table 8. The first column of Table 8 shows the values of applied axial forces in experiments, and the third column lists measured first natural frequencies of both bars. The last five column presents measured first mode shapes at the five accelerometers attached to the bar.It can easily be observed

from Table 8 that : a) The fundamental frequency of bar 1 increases gradually and bar 2 decreases gradually with the load. b) The normalized modal values of bar 1 appear in good symmetry whereas bar 2 is not. The reason for the discrepancy is perhaps due to uneven plan loading and unsymmetry of horizontal connection, which needs further investigation.

The measured and identified axial forces of both bars are listed in Table 9 for the comparison of identification accuracy. For bar 1 and bar 2, the identified axial forces are basically consistent with axial forces measured by FBG sensors and strain gauges, which are further shown in Fig. 12(a) of bar 1 and Fig. 12(b) of bar 2.

Table 8 Table of bars' frequency and modal information under single truss load

Frequency and modal		f(Hz)	1	2	3	4	5
0 kN	bar 1	88.415	0.5325	0.8991	1	0.8932	0.5313
	bar 2	95.659	0.4152	0.8099	1	0.9054	0.5469
2.5 kN	bar 1	90.001	0.5131	0.8929	1	0.8774	0.5116
	bar 2	94.954	0.4154	0.8155	1	0.8998	0.5417
5 kN	bar 1	93.533	0.4977	0.8827	1	0.8720	0.4853
	bar 2	93.492	0.4107	0.8118	1	0.9030	0.5362
7.5 kN	bar 1	97.548	0.4733	0.8548	1	0.8650	0.5064
	bar 2	91.982	0.4126	0.8084	1	0.9068	0.5495
10 kN	bar 1	98.807	0.4830	0.8699	1	0.8594	0.4966
	bar 2	90.548	0.4131	0.8104	1	0.9046	0.5451

(a) Experiment setup   (b) Experimental bar and sensor locations

Fig. 11 Experiment setup and sensor locations

(a) Bar 1   (b) Bar 2
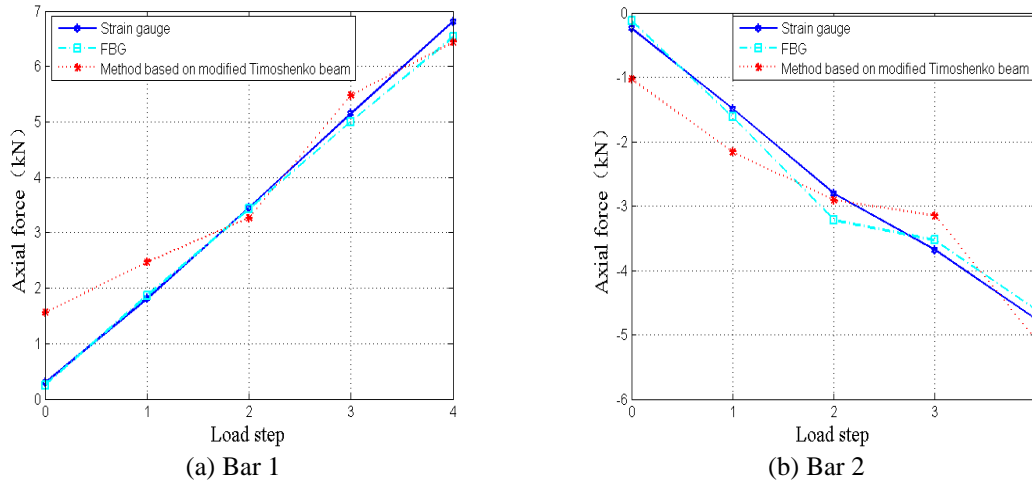
Fig. 12 Comparison of identified axial forces with measured ones by FBG sensors and strain gauges

Table 9 Table of identification axial force of two bars under single truss load

Axial force(kN)	Ways	0 kN	2.5 kN	5 kN	7.5 kN	10 kN
bar 1	FBG	0.25	1.86	3.43	5.00	6.53
	strain gauge	0.29	1.81	3.45	5.15	6.81
	improved method	1.56	2.47	3.27	5.48	6.44
bar 2	FBG	-0.12	-1.62	-3.22	-3.53	-4.62
	strain gauge	-0.24	-1.49	-2.81	-3.68	-4.76
	improved method	-1.03	-2.16	-2.91	-3.15	-5.08

In Fig. 12, the blue solid line represents measured axial forces by strain gauges, the cyan dash-dotted line represents measured axial forces by FBG sensors, and the red dotted line represents identified axial forces by the proposed method. For the loading case of 0 kN and 2.5 kN, the errors of axial force estimation are comparatively larger than measured other cased, which may be induced by initial friction effects of the connecting parts of screw and spherical hinges. For the case of 5 kN, 7.5 kN and 10 kN, the axial forces identified with the modified Timoshenko beam theory are in good agreement with FBG and strain gauge. These tests powerfully demonstrate that axial forces can be accurately identified by on the proposed modified Timoshenko beam theory, and can be further applied to actual engineering structures.

6. Conclusions

Based on modified Timoshenko beam theory, an improved method has been developed to estimate the axial force in a bar member. The method takes bending stiffness effects, rotational

inertia, shear deformation and the rotational inertia caused by shear deformation into consideration. The deformation coefficient which accounts for rotational inertia effects of the shearing deformation is extensively discussed in the paper. It is found that varying wave speed should be used for the calculation of the deformation coefficient, especially in the low frequency domain, A significant feature of the proposed method is that the axial force can be identified without assumption of the boundary conditions as conventional methods.

Consistent stiffness and mass matrices are derived based on the modified Timoshenko beam theory, and they are used in the numerical simulations to verify the accuracy and applicability of this proposed method with various boundary conditions and non-dimensional bending influence parameter ξ. Conventional Euler-Bernoulli beam theory failed for some cases, especially for cases when ξ is larger than 50, whereas the modified Timoshenko beam theory can still yield accurate axial force estimation. Consequently, the proposed method has a wider range of applicability.

Experiments on a steel plate were conducted to verify the proposed axial force identification method. With identified mode shapes and modal frequencies, axial forces are accurately identified and the error is less than 5% for most cases. The applicability of the proposed method is further verified by identifying axial forces of two bars of a steel truss. The identified axial forces are in good agreement with axial forces measured by FBG sensors and strain gauges in most cases.

The accuracy of modal identification may contribute to the accuracy of estimate axial force. How to combine identified axial forces with different modes to improve identification accuracy needs further investigations.

Acknowledgements

References

Barnes, M.R. (2009), "Form finding and analysis of tension structures by dynamic relaxation", *Int. J. Space Struct.*, **14**(2), 89-104.

Chen, L., Song, J. and Zhang, Q. (2008), "Theory and engineering practice research on cable tension measurement with EM method ", *Constr. Technol.*, (in Chinese), **37**(5), 144-153.

Chen, R., Wan, C.F. and Xue, S.T. (2005), "The correction and effect of equation of the Timoshenko beam motion", *J. Tongji university: natural science edition*, **33**(6), 711-715.

Friedman, Z. and Kosmatka, J.B. (1993), "An improved two-node Timoshenko beam finite element", *Comput. Struct.*, **47**(3), 473-481.

Greening, P.D. and Lieven, N.A.J. (2003), "Identification and updating of loading in frameworks using dynamic measurements", *J. Sound Vib.*, **260**(1), 101-115.

Irvine, H.M. and Irvine, H.M. (1992), Cable structures (Vol. 5), New York: Dover Publications.

Irvine, M. (1978), "Free vibrations of inclined cables", *J. Struct. Div. - ASCE*, **104**(2), 343-347.

Jeanlouis, Guyader. (2006), "Vibrations in Continuous Media", Library of Congress Cataloging-in-Publication Data.

Li, H.N., Li, D.S., Ren, L., Yi, T.H., Jia, Z.G. and Li, K.P. (2016), "Structural health monitoring of innovative civil engineering structures in Mainland China", *Struct. Monit. Maint*., **3**(1), 1-32.

Li, H.N., Yi, T.H., Ren, L., Li, D.S. and Huo, L.S. (2014), "Reviews on innovations and applications in structural health monitoring for infrastructures", *Struct. Monit. Maint*., **1**(1), 1-45.

Li, S., Reynders, E. Maes, K. and De Roeck, G. (2013), "Vibration-based estimation of axial force for a beam member with uncertain boundary conditions", *J. Sound Vib*., **332**(4), 795-806.

Maes, K., Peeters, J., Reynders, E., Lombaert, G. and De Roeck, G. (2013), "Identification of axial forces in beam members by local vibration measurements", *J. Sound Vib*., **332**(21), 5417-5432.

Maes, K., Reynders, E., De Roeck, G. and Lombaert, G. (2011), "Determination of axial forces by local vibration measurements", Master's Thesis, Department of Civil Engineering, KU Leuven.

Mehrabi, A.B. and Tabatabai, H. (1998), "Unified finite difference formulation for free vibration of cables", *J. Struct. Eng. -ASCE*, **124**(11), 1313-1322.

Minardo, A., Coscetta, A., Porcaro, G., Giannetta, D., Bernini, R. and Zeni, L. (2014), "Distributed optical fiber sensors for integrated monitoring of railway infrastructures", *Struct. Monit. Maint*., **1**(2), 173-182.

Peeters, B. and De Roeck, G. (2001), "Stochastic system identification for operational modal analysis: a review", *ASME J. Dynam. Syst., Meas. Control*., **123** (4) 659–667.

Reynders, E."System identification methods for (operational) modal analysis: review and comparison, Archives of Computational Methods in Engineering", **19**(1) 51-124.

Russell, J.C. and Lardner, T.J. (1998), "Experimental determination of frequencies and tension for elastic cables", *J. Eng. Mech. –ASCE* , **124**(10), 1067-1072.

Stephen, N.G. (2006), "The second spectrum of Timoshenko beam theory–Further assessment", *J. Sound Vib*., **292**(1-2), 372-389.

Su, X. (2006), "Application of MTS810 for Evaluating Mechanical Property of Ceramics", Modern Scientific Instruments.

Tullini, N. and Laudiero, F. (2008). "Dynamic identification of beam axial loads using one flexural mode shape", *J. Sound Vib*., **318**(1), 131-147.

Wang, J. and Yang, Q.S. (2017), "Sensor selection approach for damage identification based on response sensitivity", *Struct. Monit. Maint*., **4**(1), 53-68.

Williams, F.W. and Wittrick, W.H. (1970), "An automatic computational procedure for calculating natural frequencies of skeletal structures", *Int. J. Mech. Sci*., **12**(9), 781-791.

Yamagiwa, I. Utsuno, H. Endo, K. and Sugii, K. (1999), "Application of simultaneous identification of tension and flexural rigidity at once to the bridge cables", *Proceedings of the IABSE Conference, Cable-Stayed Bridges*, Past, Present, and Future.

Zui, H. Hamazaki, Y. and Namita, Y. (2002), "Study on tension and flexural rigidity identification for cables having large ratio of the diameter and the length", *Doboku Gakkai Ronbunshu*, **2002**(703), 141-149.

TY